Atmospheric Research 213 (2018) 437–449

Contents lists available at ScienceDirect

Atmospheric Research

journal homepage: www.elsevier.com/locate/atmosres

Validation of CHIRPS precipitation dataset along the Central Andes of Argentina

Juan A. Rivera[a,b,*], Georgina Marianetti[b], Sofía Hinrichs[b]

[a] Instituto Argentino de Nivología, Glaciología y Ciencias Ambientales (CCT-Mendoza/CONICET), Av. Ruiz Leal s/n, Parque General San Martín, Mendoza 5500, Argentina

[b] Facultad de Ciencias Veterinarias y Ambientales, Universidad Juan Agustín Maza. Av. Acceso Este, Lateral Sur 2245, Guaymallén, Mendoza 5519, Argentina

ARTICLE INFO

Keywords:
CHIRPS
Remote sensing
Precipitation
Spatio-temporal validation
Argentina
Andes

ABSTRACT

A validation covering a 30-year period (1987–2016) of the relatively new CHIRPS precipitation dataset was performed over the Central Andes of Argentina (CAA), a semi-arid region with complex topography and sparse ground observations. Precipitation data from 57 rain gauges and several well-known continuous and categorical validation statistics were assessed to evaluate the performance of CHIRPS estimations. The study area was divided into two zones based on the timing of the rainy season maximum, in order to determine regional differences in the characterization of precipitation patterns. The results of this study indicate that CHIRPS data reproduce adequately several characteristics of precipitation along the study area, as the seasonal and interannual variability and the spatial patterns of precipitation. CHIRPS dataset is able to capture the rainy season characteristics over the CAA, considering the Mediterranean climate features over the Andes ranges and the monsoonal regime in the lowlands. CHIRPS achieves better results for the stations located in the region with summer precipitation maximum, mostly located over Cuyo region (correlation = 0.86, bias = 11%, mean absolute error = 15.3 mm). Despite the strong correlation of 0.82 over Northern Patagonia region, CHIRPS showed a significant overestimation of the seasonal precipitation totals during the cold semester (April to September, bias = 65.8%, mean absolute error = 34.7 mm). These systematic errors can be attributed to the poor performance of CHIRPS in reproducing the precipitation features over the zones above 1000 m.a.s.l. One of the reasons behind the observed differences can be attributed to the limited number of anchor stations used in the CHIRPS calculation procedure, which highlights this study as an independent validation given the amount of meteorological stations used.

1. Introduction

The knowledge of precipitation variability, both in time and space, is crucial for water management strategies, environmental monitoring, agricultural practices and climate studies. Precipitation is one of the main input to hydrological models and to most of the indices used for flood and drought monitoring. The impacts of precipitation variability, associated to floods and droughts, often led to adverse economic effects, particularly in regions that rely on agriculture or hydropower generation. Changes in precipitation patterns can have profound societal consequences, directly affecting ecological systems, food security, disaster management and human lifes (Farooq Iqbal and Athar, 2018; Maidment et al., 2015; Thiemig et al., 2012). Thus, it is of paramount importance to provide accurate precipitation information, considering a climatological perspective based on past information, a current perspective based on operational monitoring and a future perspective based on reliable precipitation forecasts.

To achieve these goals, until some decades ago, the use of conventional rain gauge networks have provided the main source of relatively accurate point measurements of precipitation (Feidas, 2010; Katsanos et al., 2016a). However, estimations from rain gauges over mountainous areas with complex topography are often subjected to large uncertainties due to the lack of accessibility to the rain gauges –which habitually have an uneven and sparse distribution-, the limited sampling area of the gauges, and the maintenance costs of the network (Farooq Iqbal and Athar, 2018; Feidas, 2010; Zambrano-Bigiarini et al., 2017). In South America, the available rainfall network has significant limitations in its infrastructure, maintenance, density and frequency of observations (Hobouchian et al., 2017). Particularly in Argentina, to obtain accurate precipitation estimations based on rain gauges is a

* Corresponding author at: Instituto Argentino de Nivología, Glaciología y Ciencias Ambientales (CCT-Mendoza/CONICET), Av. Ruiz Leal s/n, Parque General San Martín, Mendoza 5500, Argentina.
E-mail address: jrivera@mendoza-conicet.gob.ar (J.A. Rivera).

https://doi.org/10.1016/j.atmosres.2018.06.023
Received 29 January 2018; Received in revised form 2 June 2018; Accepted 27 June 2018
Available online 02 July 2018

challenging task due to the extension of the country, the sparse distribution of the stations and the complex topography that includes the Andes, the most important mountain range in the Southern Hemisphere. In turn, 40% of the Argentinean meteorological network was lost during the 1970s, particularly after 1976 (Boulanger et al., 2010; Tencer et al., 2011), and most of the rain gauges located along the adjacencies of the Andes were dismantled (Viale and Nuñez, 2011).

To overcome these limitations, satellite-based estimates are widely used to measure precipitation given that provides quasi-global coverage, high resolution, frequent sampling and easy access (Tang et al., 2015). Satellite derived precipitation data can support the study of precipitation patterns at different temporal and spatial scales, and are a crucial tool for hydrological applications, water management and decision-making (Hobouchian et al., 2017; Mantas et al., 2015). The remarkable capabilities of satellite estimations demanded constant advancement and development of new algorithms and methods for further improving the quality of precipitation estimates (Ahmadalipour et al., 2017). Moreover, temporal and spatial resolutions are continuously improving owing to steady advances in sensor technology and new methods for merging various data sources (Thiemig et al., 2012).

Nowadays, several high-resolution products based on satellite precipitation estimates are freely available at an operational stage, differing in terms of design objective, data sources, spatial resolution, spatial coverage, published temporal resolution, temporal span and latency (Beck et al., 2017). However, the use of these databases for climate studies is only possible if precipitation estimations resemble the spatial and temporal variability based on rain gauges observations. In this sense, validations of satellite-based precipitation products are necessary to ascertain the accuracy of precipitation estimates on various spatial and temporal scales and to establish the direct usability of these products (Feidas, 2010). The validation activity has two aims: 1) to help technique developers to improve their algorithms and 2) to provide the potential users with a reliable error structure of the precipitation products (Porcù et al., 2014). Performance of different satellite products, typically evaluated comparing them to ground measurements, is different in different geographical regions, surface conditions and season (Hobouchian et al., 2017; Rahmawati and Lubczynski, 2017), which often lead to substantial biases and stochastic errors that need to be reduced or corrected before transforming the satellite estimations into operational tools with potential hydrological application (Tang et al., 2015; Thiemig et al., 2012).

Scientists at the United States Geological Survey (USGS), working closely with collaborators at the University of California, Santa Barbara Climate Hazards Group, have developed a quasi-global (50°S–50°N, 180°E–180°W), 0.05° resolution, 1981 to near-present gridded precipitation time series: the Climate Hazards Group InfraRed Precipitation with Stations (CHIRPS) data archive (Funk et al., 2014, 2015a). The CHIRPS dataset is a new land-only climatic database of precipitation, made available since early 2014; it encompasses three diverse types of information: global climatologies, satellite estimates and in situ observations (Katsanos et al., 2016b). The CHIRPS precipitation data set blends in more station data than other products and uses a high-resolution background climatology, providing better estimates of precipitation means and variations, resulting in a better hydrologic state (Shukla et al., 2014).

The CHIRPS dataset has been subjected to diverse evaluations worldwide, although the number of studies is still limited. Shukla et al. (2014) used CHIRPS estimations to generate seasonal soil moisture forecasts for agricultural drought prediction over the equatorial East Africa. Over the same region, Vigaud et al. (2017) analyzed precipitation composites based on CHIRPS to identify teleconnections with tropical Pacific surface temperatures and regional atmospheric circulation. Maidment et al. (2015) quantified the recent observed trends in precipitation over Africa with 8 gridded gauge-only and satellite-based datasets, including CHIRPS estimations. The authors observed that CHIRPS show relatively small deviations from the Climate Research Unit (CRU) gauge analysis. Le and Pricope (2017) used the CHIRPS dataset into a standard hydrologic model for the simulation of streamflow over Western Kenya. A meteorological drought assessment over Southeast Asia was performed by Guo et al. (2017) using the CHIRPS estimations to calculate the standardized precipitation index (SPI, McKee et al., 1993). Katsanos et al. (2016a) analyzed precipitation extremes based on CHIRPS over Cyprus, after a validation study that allowed to identify a trend in the difference between rain gauges and CHIRPS over time (Katsanos et al., 2016b). The first quasi-global evaluation of CHIRPS dataset was performed by Beck et al. (2017), finding that CHIRPS presents a viable choice for tropical regions.

This dataset was recently considered for validation studies over South America. Particularly, Funk et al. (2015a) evaluated CHIRPS during the rainy season in areas of complex terrain as Colombia and Peru. They obtained that CHIRPS estimations were comparable to the variability of the Global Precipitation Climatology Centre (GPCC) dataset. Paredes-Trejo et al. (2016) performed a validation of CHIRPS over Venezuela, finding an acceptable overall performance but with a low skill of rain detection, which prevents its use for agricultural purposes. Over Northeastern Brazil, CHIRPS arise as a promising tool for drought monitoring, performing better outside the semi-arid region, although rain detection is deficient over the studied domain (Paredes-Trejo et al., 2017). This product has been recommended for (quasi-) real-time monitoring and hydrological applications over Chile (Zambrano-Bigiarini et al., 2017). Nevertheless, Zambrano et al. (2017) showed that the product should be calibrated to adjust to rainfall especially over northern Chile.

The Central Andes of Argentina (CAA) is a region where the interplay between the complex topography and the atmospheric circulation determines a wide range of precipitation features, from intense winter orographic precipitation (Viale and Norte, 2009), extreme summer precipitation events leading to the occurrence of landslides along the Andes (Santos et al., 2015) and hailstorms over the lowlands (Biles and Cobos, 2007), to multi-annual severe drought events (Penalba and Rivera, 2016; Rivera et al., 2017). In view of the lack of observations over the region, it is crucial to advance in the understanding of precipitation variability at diverse spatial and temporal scales by using available satellite-derived precipitation databases, considering the large negative impacts associated to precipitation variations on agriculture and water resources sectors.

The aim of this study is to assess the accuracy of monthly CHIRPS satellite-based estimations along the CAA, in order to quantify its suitability to represent the spatial patterns of precipitation, its seasonality and interannual variability. To our best knowledge, given the long-record −1981 to near present- of CHIRPS estimations, this will be the validation of a satellite-based precipitation product over the longer period of time ever performed in the region. Thus, the outcomes of this study will be a baseline for the study of climate variability and change, the assessment of precipitation at small-catchment scale and the development of meteorological, agricultural and hydrological drought monitoring tools over the CAA. This paper is organized as follows: Section 2 presents the study area, the rain gauge data used, the CHIRPS dataset and the validation statistics. Section 3 presents the results of the precipitation intercomparison. The discussion of the main findings is presented in Section 4, while the conclusions are summarized in Section 5.

2. Study area and data sources

In this study, the CAA was defined as the Argentinean sector of the region located between 30°-40°S and 67°-71°W (Fig. 1). The study area spans part of two geographical regions of the country: Cuyo region (30°-36°S, comprising the provinces of San Juan and Mendoza, where the Andes have a mean elevation of 3500 m) and northern Patagonia region (36°S-40°S, comprising Neuquén province, where the mean elevation of the Andes decrease to 1500 m). The Andes ranges strongly affect the

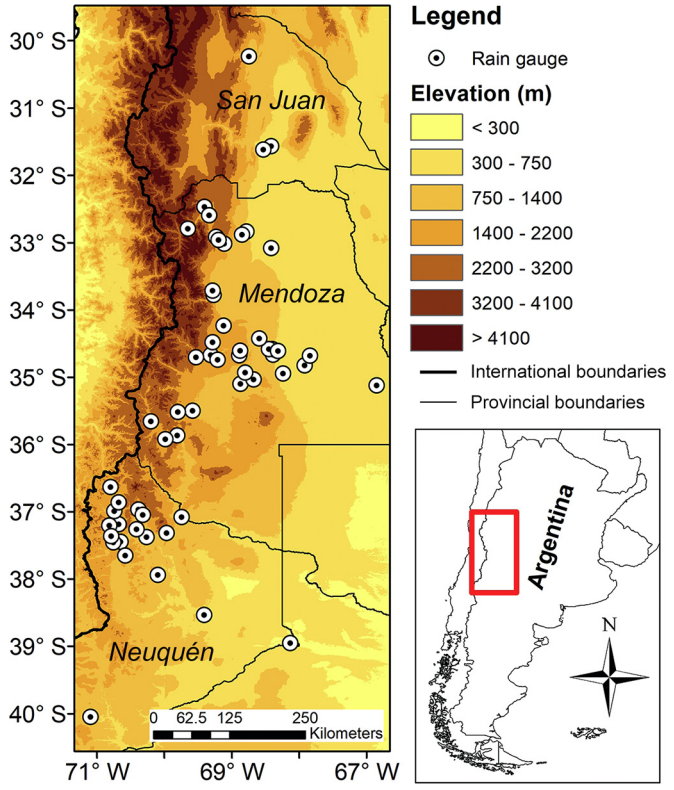

Fig. 1. Location of the study area with the main topographic features and the rain gauges used for the validation of satellite-based estimates.

regional precipitation patterns over these regions, through interactions with the continental atmospheric circulation and the incursion of moist air masses from the Pacific Ocean (Rivera et al., 2017). Along the study area, the Andes act as a permanent barrier to the humid air masses from the mid-latitude South Pacific Ocean and the baroclinic precipitation systems coming from the west. The climate at high elevations has a Mediterranean regime with higher precipitations during the cold season (April to September) and dry warm seasons (October to March), in response to the seasonal displacement of the South Eastern Pacific High (Falvey and Garreaud, 2007). Over this area precipitation is mainly generated by the passage of cold fronts moving eastward from the Pacific (Garreaud, 2009). Due to the strong rain shadow effect, climate east of the Andes is arid to semi-arid, where convective warm season rainfalls favored by moist air masses from the Amazon and Atlantic basins play a relevant role (Schwerdtfeger, 1976). There are very intense storms east of the Andes during the warm season, capable to develop large hail over the study area (Biles and Cobos, 2007).

The CAA is the major wine producer region in Argentina, and the agro-industrial activities in CAA depend largely on grape production, an activity only possible through irrigation. Dams and reservoirs collect the snowmelt contribution to the streamflows during the warm season. Along Cuyo region, 95% of its 2.5 million inhabitants are distributed just within the 4% of the territory, highlighting the vulnerability of the region to periods of water shortages. Regarding Northern Patagonia, the rivers which are born in the higher elevations of the Andes, fed by snowmelt and rainfall, play an important role in the development of the region, with several hydropower plants providing a significant part of the electric power in Argentina (Seoane et al., 2005).

2.1. Rain gauge observations

Initially, monthly precipitation records from 103 rain gauges were collected from the National Weather Service (Servicio Meteorológico Nacional, SMN) and the Water Resources Agency of Argentina (Subsecretaría de Recursos Hídricos, SSRH; http://bdhi.hidricosargentina.gob.ar/) databases. A filtering method was used to select the time series with < 15% of missing data, with a data length requirement of at least 30 years, comprising ideally the most recent

Table 1
Geographical characteristics and percentage of missing data of the selected rain gauges for the 1987–2016 period.

Name	Province	Lat (°S)	Lon (°W)	Elevation (masl)	Source	Missing data (%)
San Juan	San Juan	31.57	68.42	598	SMN	2.22
San Juan INTA	San Juan	31.62	68.53	603	SMN	3.88
Jachal	San Juan	30.23	68.75	1175	SMN	3.88
San Martín	Mendoza	33.08	68.42	653	SMN	0.00
Mendoza Aero	Mendoza	32.83	68.78	704	SMN	0.00
Mendoza Observatorio	Mendoza	32.88	68.85	827	SMN	0.00
Malargüe	Mendoza	35.50	69.58	1425	SMN	0.00
San Rafael	Mendoza	34.58	68.40	748	SMN	0.00
La Angostura	Mendoza	35.09	68.87	1302	SSRH	0.00
La Jaula	Mendoza	34.67	69.32	1457	SSRH	0.00
Rama Caída	Mendoza	34.67	68.38	714	SSRH	1.67
El Nihuil	Mendoza	35.03	68.67	1309	SSRH	0.00
Villa Atuel	Mendoza	34.82	67.92	519	SSRH	0.00
Capitán Montoya	Mendoza	34.58	68.45	820	SSRH	3.33
Las Salinas	Mendoza	34.93	68.81	1320	SSRH	5.56
Puesto Canales	Mendoza	34.67	68.89	1574	SSRH	0.00
Puesto Carmona	Mendoza	34.68	67.84	522	SSRH	0.00
Arroyo Hondo	Mendoza	34.48	69.28	1900	SSRH	0.00
Las Aucas	Mendoza	34.70	69.54	1800	SSRH	1.67
Las Malvinas	Mendoza	34.94	68.24	602	SSRH	0.00
Los Mayines	Mendoza	35.66	70.20	1663	SSRH	2.50
Bardas Blancas	Mendoza	35.87	69.81	1445	SSRH	1.67
Arroyo La Vaina	Mendoza	35.92	69.99	1550	SSRH	1.67
Puesto Las Moras	Mendoza	35.12	66.85	388	SSRH	0.00
Cacheuta	Mendoza	33.01	69.12	1250	SSRH	6.39
Guido	Mendoza	32.92	69.24	1408	SSRH	0.28
Valle de Uco	Mendoza	33.78	69.27	1199	SSRH	1.67
Pincheira	Mendoza	35.52	69.81	1775	SSRH	7.50
San Rafael	Mendoza	34.61	68.32	681	SSRH	0.28
Las Vertientes	Mendoza	34.42	68.59	990	SSRH	1.11
Juncalito	Mendoza	34.74	69.21	1593	SSRH	4.72
Puesto Morales	Mendoza	34.60	68.87	1455	SSRH	0.83
Polvaredas	Mendoza	32.79	69.65	2250	SSRH	0.28
Potrerillos	Mendoza	32.96	69.20	1427	SSRH	1.11
Puesto Papagayos	Mendoza	34.23	69.12	1529	SSRH	3.05
La Remonta	Mendoza	33.71	69.29	1360	SSRH	0.28
San Alberto	Mendoza	32.47	69.41	2180	SSRH	14.44
Uspallata	Mendoza	32.59	69.34	1890	SSRH	3.33
Buta Ranquil	Neuquén	37.07	69.75	816	SSRH	0.28
Paso de Indios	Neuquén	38.53	69.41	498	SSRH	5.56
El Cholar	Neuquén	37.44	70.65	1230	SSRH	5.83
Chos Malal	Neuquén	37.37	70.27	856	SSRH	2.78
Andacollo	Neuquén	37.18	70.68	1011	SSRH	12.22
Junín de los Andes	Neuquén	40.05	71.10	750	SSRH	9.44
Vilu Mallín	Neuquén	37.46	70.76	1065	SSRH	1.67
Cajón Curileuvú	Neuquén	36.96	70.39	1400	SSRH	4.17
El Alamito	Neuquén	37.26	70.42	1032	SSRH	5.28
Las Ovejas	Neuquén	36.98	70.75	1267	SSRH	2.78
Varvarco	Neuquén	36.86	70.68	1180	SSRH	3.61
El Huecu	Neuquén	37.65	70.58	1212	SSRH	1.67
Tricao Malal	Neuquén	37.04	70.32	1350	SSRH	0.00
Los Miches	Neuquén	37.21	70.82	1219	SSRH	0.83
Chochoy Mallín	Neuquén	37.36	70.79	1066	SSRH	1.94
Chorriaca	Neuquén	37.94	70.10	1100	SSRH	7.22
Pichi Neuquén	Neuquén	36.63	70.80	1350	SSRH	0.83
Auquinco	Neuquén	37.32	69.97	1520	SSRH	2.22
Neuquén	Neuquén	38.95	68.13	271	SMN	0.00

period of records. After these procedures, the final database consisted on monthly precipitation observations from 57 stations (see Fig. 1) with measurements over the 1987–2016 period. In addition, the names and relevant particulars of the selected rain gauges are summarized in Table 1. As can be observed in Fig. 1, the region has scarcely available meteorological data for a long-term climatic assessment, particularly considering the stations from the SMN (Table 1). Precipitation time series were subjected to quality control procedures, considering the techniques applied by González (2013) to the time series over the study area. Moreover, we analyzed the spells of months without precipitation, removing from the assessment the periods larger than 5 months, a threshold identified by Llano and Penalba (2011) over the study area based on high-quality precipitation time series. Reasons behind the occurrence of these long spells can be attributed due to the inaccessibility to the stations mainly during winter months. Extreme precipitation totals were also analyzed considering the spatial distribution of precipitation in the nearest rain gauges, in the cases were monthly totals exceeded four times the standard deviation above the mean. This criteria has been previously used by Penalba et al. (2014) considering daily precipitation totals and is in line with the threshold level used by Paredes-Trejo et al. (2016, 2017) for monthly data. Additionally, homogeneity control using the Standard Normal Homogeneity Test (Alexandersson, 1986) for a confidence level of 95% allowed to identify inhomogeneities in just 6 of the 57 precipitation time series. These inhomogeneities were not corrected given that occurred during the first or the last year of record. Missing data were replaced by applying linear regressions with neighboring stations, only for reference stations that explain > 80% (R^2 > 0.8) of the temporal behavior of precipitation. Even when the final set of precipitation time series still have some missing months –either because of removal of suspicious records or to the lack of close reference stations to fill missing gaps- this aspect is not expected to affect the comparability of the results or the calculation of the metrics for CHIRPS comparison.

2.2. CHIRPS precipitation estimates

The CHIRPS monthly precipitation product was obtained through the Climate Hazards Group (CHG) of the University of California at Santa Barbara (UCSB) webpage (http://chg.geog.ucsb.edu/data/chirps/index.html) for the years 1987–2016, which overlaps the period of ground-based precipitation data. This dataset is updated at near-real time, has quasi-global coverage (land only, 50°S-50°N) with a spatial resolution of 0.05° (approximately 5 Km) and several temporal scales (monthly, decadal, pentadal or daily time steps). The CHIRPS dataset was produced blending precipitation estimates based on infrared cold cloud duration (CCD) observations calibrated using Tropical Rainfall Measuring Mission (TRMM) Multi-Satellite Precipitation Analysis (MSPA) with in-situ station data from a variety of sources including national and regional meteorological services (see Funk et al., 2014, 2015a, 2015b for details). The incorporation of station data also helps to correct for estimates that often underestimate the intensity of precipitation events (Le and Pricope, 2017). This relatively new product was designed for drought monitoring in places with complex topography, changing observation networks and deep convective precipitation systems (Funk et al., 2015b), features that are present in the study area. Moreover, the spatial resolution of CHIRPS is higher than other satellite-based global precipitation datasets, making it favorable to analyze precipitation variations at small basin scales.

The temporal evolution of the anchor stations used in the creation of CHIRPS over the study area is presented in Fig. 2 for the 1987–2016 period. Between 2 and 12 anchor stations were used, all of them provided by the SMN and obtained through either the Global Historical Climate Network (GHCN) or the Global Summary of the Day (GSOD), as can be observed in ftp://ftp.chg.ucsb.edu/pub/org/chg/products/CHIRPS-2.0/diagnostics/monthly_station_data/. This temporal evolution shows a large decadal variability, with an average of 11 stations during the last part of 1980s, 6 stations during the 1990s and 8 between 2000 and 2016 (Fig. 2). Starting with the national datasets, the list of anchor stations to create CHIRPS were increased adding regional and global sources (Funk et al., 2014). Nevertheless, the incorporation of a valuable national source as the SSRH was discarded, perhaps given the hydrological focus of the rain gauges information of this dataset or the lack of knowledge about its existence and availability. As can be observed in Table 1, just 9 of the 57 rain gauges used for this validation where provided by the SMN, which indicates that the incorporation of data from the SSRH could result in an improvement of CHIRPS estimations over the study area and, particularly, over Argentina. Moreover, just one of the anchor stations was located in Neuquén province, with two of the anchor stations having a precipitation maximum during the cold semester (Neuquén and Malargüe stations). Considering this limitation, the validation of CHIRPS precipitation dataset over the CAA it can be considered as an independent validation.

3. Methodology

3.1. Continuous validation statistics

A point-to-pixel analysis was performed to compare the time series of rain gauges observations to the corresponding CHIRPS pixel. This comparison allows capturing the small scale variability of monthly precipitation totals (Thiemig et al., 2012), largely subjected to its seasonality and the topography of the study area. Therefore, we selected the CHIRPS estimations for the 57 grid points conrresponding to the location of the rain gauges. An interpolation of the observed precipitation would involve large uncertainties given the lack of a high-density rain gauges database to reproduce adequately the precipitation gradients along the complex terrain, although this alternative was previously carried out over the study area (Hobouchian et al., 2017) and other regions of the world (Dinku et al., 2008; Feidas, 2010).

To evaluate the performance of CHIRPS in estimating the amount of the precipitation we used the following comparison statistics: the Pearson correlation coefficient (PCC), the mean absolute error (MAE), the Nash-Sutcliffe efficiency (NSE) and the percent bias (PB) (Table 2). The PCC measures the linear relationship strength between the satellite estimations and the rain gauges observations, bounded by −1 and 1 with an optimal value of 1. The MAE provides information on the average magnitude of error estimations, considering both systematic and random errors. Several studies are replacing the widely used root mean squared error (RMSE) by the MAE because the errors are unlikely to be unbiased or to follow a normal distribution (Beck et al., 2017; Willmott et al., 2017). The perfect score for this statistic is 0. The NSE (Nash and Sutcliffe, 1970) determines the relative magnitude of the variance of the residuals compared to the variance of the observed values of precipitation. This statistic vary from minus infinity to 1, being negative in cases of poor precipitation estimation and an optimal value equal to 1, which would indicate that the estimated values matched observed precipitation exactly. The PB measures the average tendency of the estimated precipitation to be larger or smaller than the observed precipitation, with an optimal value of 0. Positive values indicate overestimation bias, whereas negative values indicate underestimation bias.

3.2. Systematic and random error components

Characterizing satellite precipitation errors and their random and systematic components is essential to develop bias reduction techniques, and thus to improve precipitation retrieval algorithms, and for many operational applications (Maggioni et al., 2016). According to Willmott (1981), the error in the numerical weather prediction models can be separated into systematic and random error components of the mean squared error (MSE):

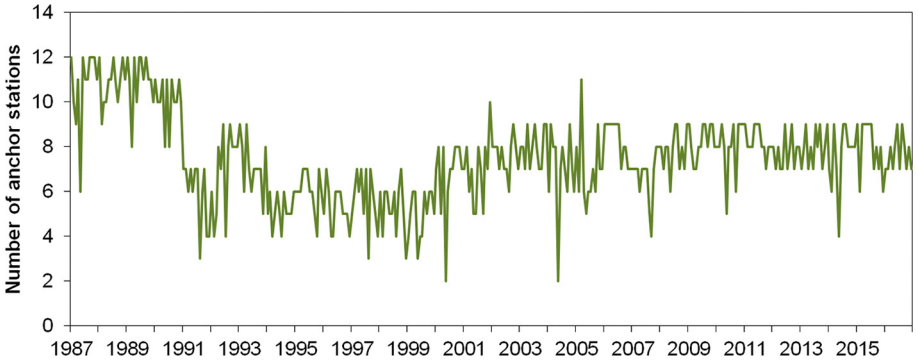

Fig. 2. Temporal evolution of the number of anchor stations used for the estimation of CHIRPS dataset within the study area for the period 1987–2016.

Table 2
Statistical measures of performance used for analysis based on continuous metrics, where: G = rain gauge observations, $\overline{G}$ = average rain gauge observations, S = CHIRPS estimations, $\overline{S}$ = average CHIRPS estimations and N = number of data pairs.

Statistic	Ecuation
Pearson correlation coefficient (PCC)	$r = \frac{\sum(G-\overline{G})(S-\overline{S})}{\sqrt{(G-\overline{G})^2}\sqrt{(S-\overline{S})^2}}$
Mean absolute error (MAE)	$MAE = \frac{1}{N}\sum(\lvert S-G\rvert)$
Nash-sutcliffe efficiency (NSE)	$NSE = 1-\frac{\sum(S-G)^2}{\sum(G-\overline{G})^2}$
Percent bias (PB)	$PB = 100\frac{\sum(S-G)}{\sum G}$

$$MSE = MSE_{Syst} + MSE_{Rand} \text{ and } \frac{\sum(S-G)^2}{N} = \frac{\sum(\widehat{S}-G)^2}{N} + \frac{\sum(S-\widehat{S})^2}{N}$$

where $\hat{S}$ is defined as

$$\widehat{S} = aS + b$$

where a and b are parameters (slope and intercept, respectively) to be calibrated. The systematic error is defined as the part of error to which a linear function can be fitted (Habib et al., 2009). Following AghaKouchak et al. (2012), the systematic and random components of error were expressed as $MSE_{Syst}/MSE \times 100$ and $MSE_{Rand}/MSE \times 100$, respectively.

3.3. Categorical validation statistics

Complementary, several categorical validation statistics were used to assess CHIRPS rain-detection capabilities. The statistics were derived from a contingency table involving four event combinations: hits (A) –months when both rain gauge and CHIRPS detect precipitation; false alarms (B) –months when CHIRPS detects precipitation and rain gauge not; misses (C) –months when rain gauge recorded precipitation and CHIRPS not; and correct negatives (D) –both rain gauge and CHIRPS detect no precipitation (see Table 3). Following the assessments of Toté et al. (2015) and Paredes-Trejo et al. (2017), we used a precipitation threshold of 5 mm.

Table 3
Contingency table for comparing rain gauge observations and satellite-based precipitation estimates (precipitation threshold used is 5 mm).

	Gauge ≥ threshold	Gauge < threshold
Satellite ≥ threshold	A	B
Satellite < threshold	C	D

Table 4
Statistical measures of performance used for analysis based on categorical metrics, where: A = number of hits, B = number of false alarms, C = number of misses, D = number of correct negatives, N = number of data pairs and Ar stands for hits that could occur by chance.

Statistic	Equation
Probability of detection (POD)	$POD = \frac{A}{A+C}$
False alarm rate (FAR)	$FAR = \frac{B}{A+B}$
Equitable threat score (ETS)	$ETS = \frac{A-Ar}{A+B+C-Ar}$ where $Ar = \frac{(A+B)(A+C)}{N}$
Hanssen-Kuipers discriminant (HK)	$HK = \frac{A}{A+C} - \frac{B}{B+D}$
Heidke skill ccore (HSS)	$HSS = \frac{2(AD-BC)}{(A+C)(C+D)+(A+B)(B+D)}$
Frequency bias index (FBI)	$FBI = \frac{A+B}{A+C}$

The validation statistics include the probability of detection (POD), the false alarm rate (FAR), the equitable threat score (ETS), the Hanssen-Kuipers discriminant (HK), the Heidke skill score (HSS) and the frequency bias index (FBI) (Table 4). The POD gives the fraction of precipitation occurrences that were correctly detected; it ranges from 0 to a perfect score of 1. The FAR gives the fraction of events for which CHIRPS detected precipitation but was not observed; ranging from 0 to 1 with a perfect score of 0. The ETS measures the fraction of observed and/or estimated events that are correctly predicted, adjusted by the frequency of hits that would be expected to occur simply by random chance. The range of ETS is $-1/3$ to 1, with a perfect score of 1, 0 for no skill and negative values indicate that chance estimation of the event should be preferred (Zambrano-Bigiarini et al., 2017). The HK shows how well the satellite estimates discriminate between precipitation and no-precipitation events; ranging from -1 to 1, with a perfect score of 1 and no skill for 0. The HSS, which ranges from minus infinity to 1, measures the accuracy of the estimates accounting for matches due to random chance. An HSS < 0 indicates that random chance is better than the satellite product, an HSS of 0 means the product has no skill, and an HSS of 1 indicates a perfect estimation of precipitation by the product (Diem et al., 2014). Finally, the FBI reveals systematic differences between precipitation events frequency in raingauge observations and CHIRPS-based precipitation estimates. It can indicate whether there is a tendency to underestimate (FBI < 1) or overestimate (FBI > 1) precipitation events, ranging from 0 to infinity with a perfect score of 1.

4. Results

4.1. Annual precipitation climatology over the Central Andes of Argentina

As a first step, the CHIRPS precipitation estimates were compared with the rain gauges observations considering the spatial distribution of

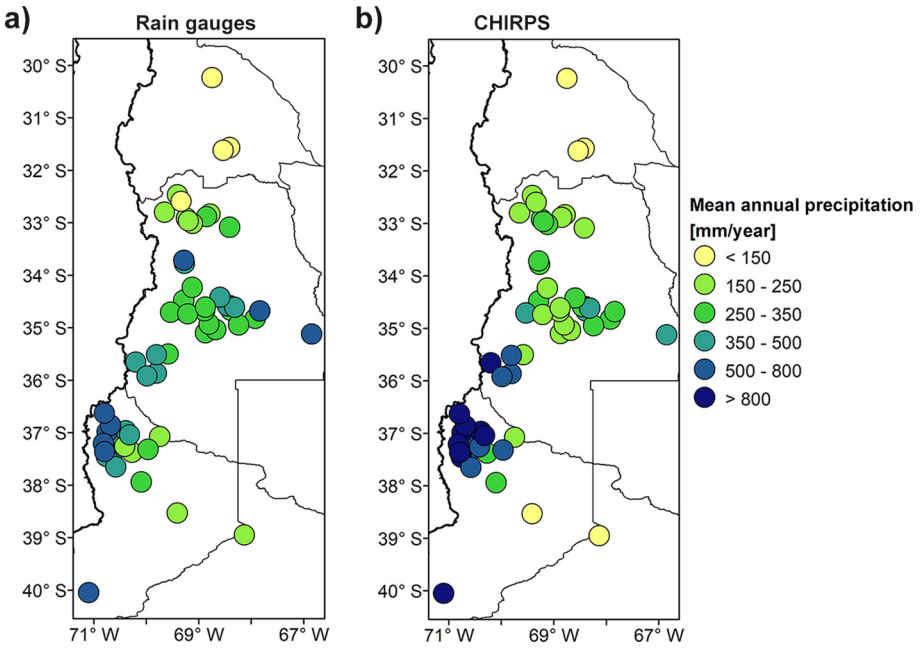

Fig. 3. Mean annual precipitation over the CAA: a) based on rain gauges observations and b) based on CHIRPS estimations.

the annual average precipitation totals over the study area. This assessment is shown in Fig. 3, considering the climatology for the 1987–2016 period. Regarding Northern Patagonia, observed precipitation ranges from over 700 mm at the high elevations of the continental divide, between 37° and 40° S, to < 300 mm east of the Andes. At these latitudes, there is a strong precipitation gradient from west to east due to the rain-shadow effect of the Andes. This spatial pattern of annual precipitation is properly reproduced by the CHIRPS estimations, although with an overestimation of the mean annual totals close to the Andes ranges and an underestimation east of the Andes, between 68° to 70° S. This feature indicates that the precipitation gradient associated to the rain-shadow effect is magnified considering the satellite estimations. In contrast to the observed 500–800 mm close to the higher elevations of the Andes, CHIRPS shows annual precipitation totals between 900 and 1300 mm (Fig. 3), while precipitation tends to be underestimated by 50 mm approximately in the lowlands of Neuquén province. Considering Cuyo region, the observations show annual precipitation totals below 150 mm over San Juan province (north of 32° S), while higher values are distributed in the central-eastern portion of Mendoza province (approximately 34° - 35° S). The mean annual CHIRPS precipitation estimates over this region show a similar spatial pattern than the observations, although some regional features are poorly captured by CHIRPS, as the relative maximum over Uco Valley (around 34° S; 69.5° W) or the annual totals over the region east of 68° W (Fig. 3). Moreover, CHIRPS estimations tend to overestimate precipitation totals over the southwestern portion of Mendoza, close to the Andes (35.5° S; 70° W), increasing the precipitation gradient as in the case of Northern Patagonia.

4.2. Annual cycle of precipitation

As previously described in Section 2, the annual cycle of precipitation shows two distinct regional features related to the atmospheric circulation over the region and its interaction with the Andes range: a Mediterranean regime close to the higher elevations of the Andes, where the average precipitation is higher in the cold season than in the warm season, and a monsoonal regime over the low lands dominated by convective warm season rainfalls and a relatively dry cold season. Fig. 4 shows some of the main features of the annual cycle of precipitation over the CAA. Firstly we classified the rain gauges according to the seasonal precipitation features, an assessment shown in Fig. 4 a. The spatial distribution of the rain gauges with higher precipitation during the warm season is restricted to the region east of 69.5° W approximately. Conversely, rain gauges west of this longitude show higher precipitation values during the cold season (Fig. 4 a). CHIRPS estimations reproduce this spatial pattern adequately, therefore highlighting its ability to discriminate the seasonal climatic features of precipitation over the CAA. Just in 6 of the 57 locations the CHIRPS estimates of the annual cycle of precipitation differed from the observations, with 5 pixels showing higher precipitations during the cold season (corresponding to the locations of Guido, La Jaula, Arroyo Hondo, Juncalito and Puesto Papagayos) and one location showing higher precipitations during the warm season (Paso de Indios), with observations showing an opposite behavior (Fig. 4 a). These stations are located in the geographical transition between the influence of the frontal systems during the cold season and the convective systems during the warm season. Hence, in this transitional region it is expected a reduction in the seasonality of precipitation.

To exemplify the seasonal precipitation variability over the region, Fig. 4 b shows the boxplots of monthly precipitation for six selected locations. There is a good agreement between rain gauges observations and CHIRPS estimations considering Mendoza Aero, Rama Caída and Chochoy Mallín time series. The seasonality of precipitation is correctly reproduced by satellite estimations, although precipitation values during the warm semester are slightly underestimated at Mendoza Aero –especially during January, February and March- and overestimated at Rama Caída –particularly during November, December, January and March- (Fig. 4 b). For these 3 sites it can be observed that the variability of precipitation during the rainy season –represented by the interquartile range- is larger than for the dry season, considering both observations and CHIRPS estimations, although CHIRPS precipitation estimates exhibit less variability than the observations particularly during the dry season. Additionally, we analyzed the performance of CHIRPS for 3 locations over the transitional region (Guido, La Jaula and Auquinco, Fig. 4 b). As shown in Fig. 4 a, CHIRPS precipitation estimations for Guido and La Jaula show that the larger precipitation totals are in the cold season, while observations indicate the opposite, although the annual cycle in precipitation is not clearly monsoonal. CHIRPS estimations show a double maximum over Guido station, with a summer peak in February and a winter peak in May and August, while

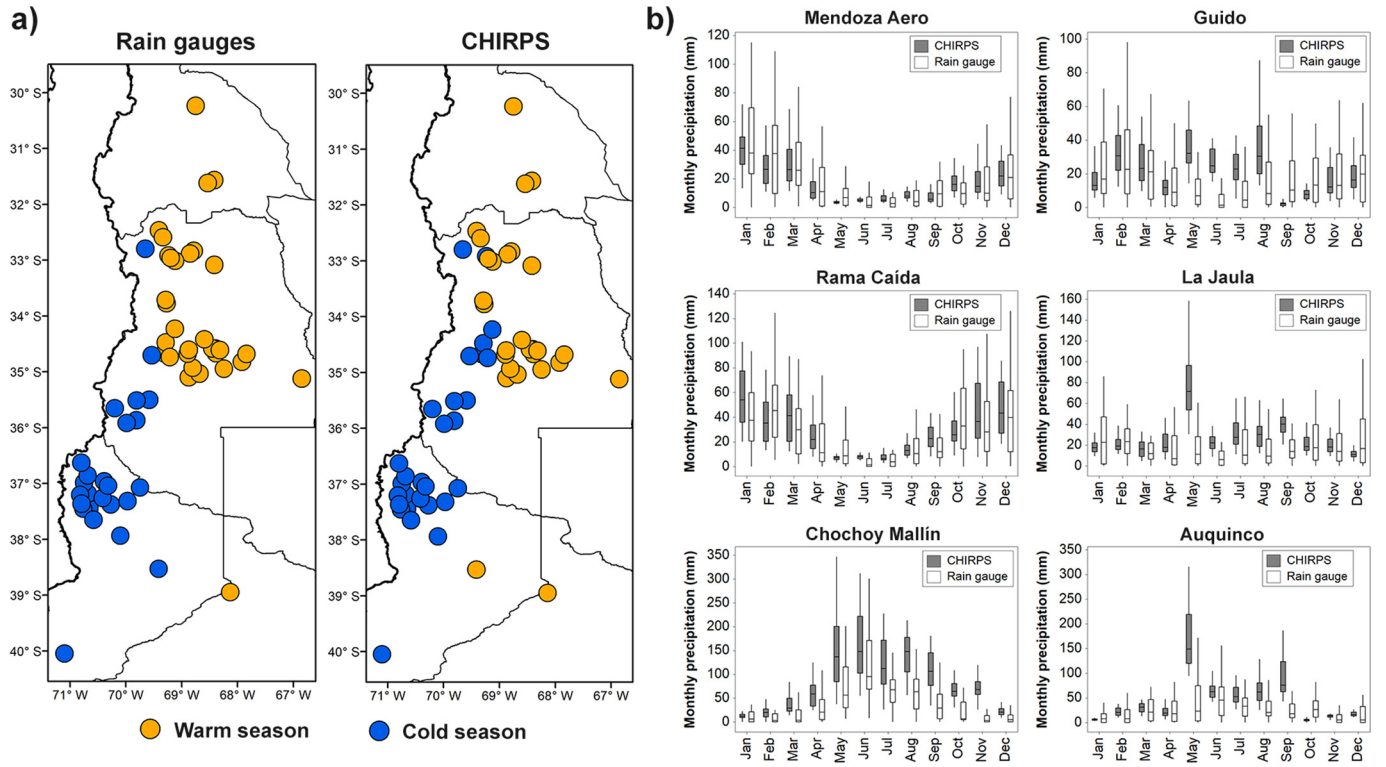

Fig. 4. a) Spatial distribution of the season of higher precipitation amounts for the 57 rain gauges and its correspondent CHIRPS pixel. b) Boxplot of the mean monthly precipitation for 6 selected stations along the CAA. Each boxplot shows the median and first and third quartiles, while the whiskers extend to the data values that are 1.5 times the interquartile range above or below the quartiles. Notice that the scale of the monthly precipitation varies among the selected stations.

observations show higher precipitations during the warm semester. Regarding La Jaula station, the seasonal variability of observed precipitation is not clearly defined. Monthly precipitation totals based on rain gauges exhibit larger variability than the estimations based on CHIRPS, with the exception of the month of May. A double maximum during the cold season is estimated by CHIRPS during May and September, a feature that is also evident at Auquinco station (Fig. 4 b), with an overestimation of precipitation totals especially during the cold season.

To further illustrate the differences in the representation of the annual cycle of precipitation, Fig. 5 shows the scatterplots of the observed precipitation and the CHIRPS estimations averaged over the rainy and dry season of each location. Considering the 57 locations, the rainy season estimations show a good agreement with the observations (PCC = 0.86), and similar results can be found considering the stations with higher precipitation during the warm season (PCC = 0.85) or the stations with higher precipitation during the cold season (PCC = 0.89). Nevertheless, CHIRPS estimations tends to show an overestimation of precipitation totals mostly over North Patagonia and southwestern Cuyo –the stations with rainy season during the cold semester-, while there is a slight underestimation considering the locations with the rainy season during the warm semester –most of Cuyo region- (Fig. 5 a). Regarding the dry season estimations, the linear regression considering the 57 locations indicates a poor agreement between observations and CHIRPS estimations (PCC = 0.27), which indicates that CHIRPS data misrepresent the precipitation totals during this season. This is particularly evident considering the stations with dry season during the warm semester (PCC = 0.15), while most of the stations located over

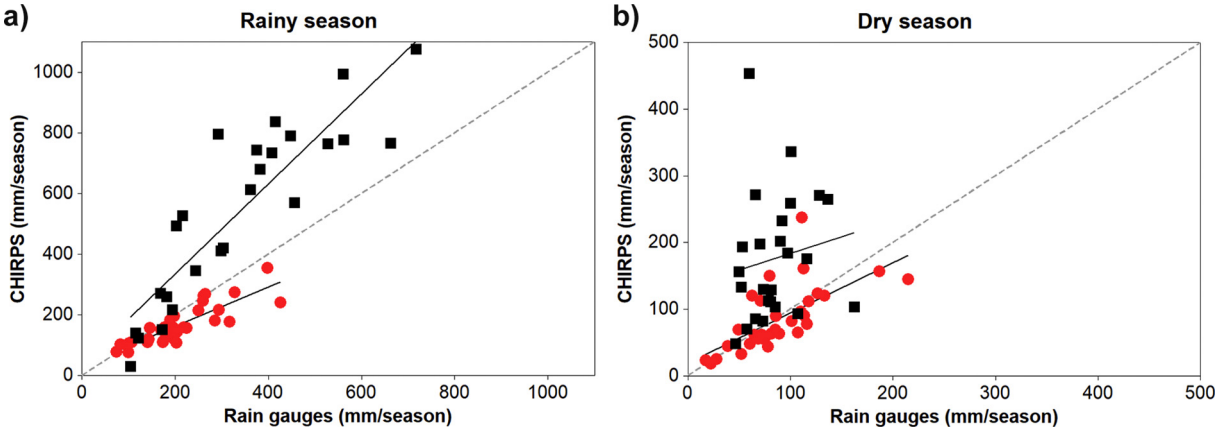

Fig. 5. a) Rainy season and b) dry season precipitation scatter plots comparing the 57 rain gauges data with the corresponding grids of CHIRPS estimations over the 1987–2016 period, with linear regression fits (black lines) for the stations showing higher precipitation totals during the cold season (squares) and the stations showing higher precipitation totals during the warm season (circles). The grey dashed line represents a 1:1 relation.

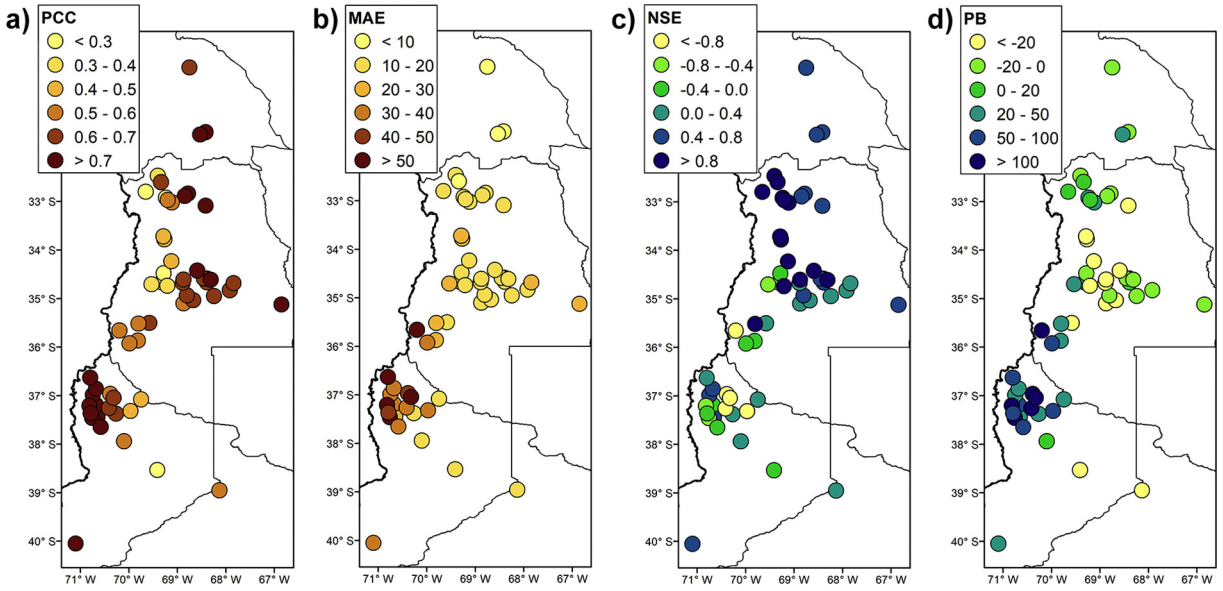

Fig. 6. Spatial distribution of the continuous statistics used to measure the agreement between observations and CHIRPS estimations: a) Pearson correlation coefficient, b) mean absolute error, c) Nash-Sutcliffe efficiency and d) percent bias.

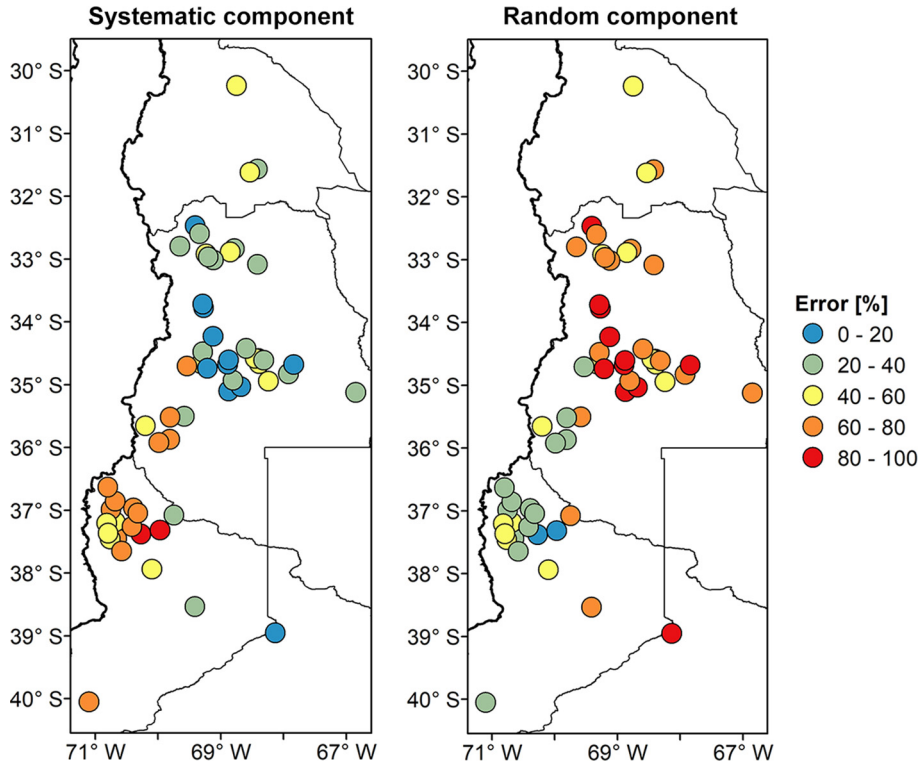

Fig. 7. Systematic and random error components (%) over the CAA for CHIRPS monthly precipitation estimations.

Cuyo region show an acceptable skill (PCC = 0.66) (Fig. 5 b). Once again, CHIRPS estimations show an overestimation of precipitation over North Patagonia, with a slight underestimation of dry season precipitation over most of Cuyo region.

4.3. Spatial distribution of continuous validation statistics

The spatial variations of the continuous statistics used for the validation of CHIRPS estimations across the CAA are shown in Fig. 6. The values of PCC show a better agreement between observations and satellite estimations close to the Andean portion of North Patagonia and in the lowlands of Cuyo region, with values higher than $r = 0.6$ (Fig. 6 a). Low correlations are observed over the mountainous region of Mendoza, particularly in the central portion of the province where the annual cycle of precipitation was poorly captured by CHIRPS. Regarding the spatial behavior of the MAE, Fig. 6 b) indicates that higher errors are located over the northwest of North Patagonia and the southwestern tip of Cuyo region, with values ranging from 30 to over 50 mm. The NSE is above 0.4 in a large portion of Cuyo region, with 16 locations with values higher than 0.65, a threshold that indicates that CHIRPS estimations are in agreement with observations (Förster et al., 2016). The NSE values decrease over North Patagonia, even with

negative values of efficiency (Fig. 6 c), in coincidence with the region where larger MAE are observed. The spatial distribution of the PB indicates that CHIRPS estimations over most of North Patagonia region tend to overestimate precipitation values, with bias larger than 20% (Fig. 6 d). Over Cuyo region the spatial pattern is heterogeneous but with a large number of locations showing an underestimation of precipitation values over the center of Mendoza province, a result previously shown in Fig. 5. The wet bias over the Andean portion of Neuquén province is in line with the poor performances considering the MAE and NSE, even when the PCC between observations and CHIRPS estimations is above 0.7. Moreover, this result is supported by Fig. 5 considering both the rainy and dry seasons. The MAE, the NSE and the PB show that the CHIRPS estimations provide a good approximation to observed precipitation over northern Cuyo region (north of 34° S), even when the PCC have low values closer to the Andes. Conversely, the Andean region of North Patagonia has large PCC but the overestimation of precipitation is translated to high MAE and low NSE.

4.4. Systematic and random errors

Fig. 7 shows the spatial distribution of the systematic and random components of error over the study area. Considering the systematic component of CHIRPS estimations, the higher values are observed over the region that showed large positive PB, high MAE and low NSE (see Fig. 6), located south of 35° S and west of 69° W (Fig. 7). As observed in Fig. 4, the overestimation of precipitation over this region, especially in the winter, and the misrepresentation of the dry season totals can be factors that contribute to the systematic error. The areas with low systematic error can be associated with the blending procedure using rain gauges measurements, given that the spatial pattern resembles the distribution of the anchor stations used for CHIRPS estimations (not shown). Over this region, the systematic component is less than the random error component (Fig. 7) and corresponds to the areas with low MAE, PB and high NSE (see Fig. 6).

4.5. Performance based on categorical validation statistics

To measure algorithm performance for different rain rates it is useful to plot the categorical scores as a function of an increasing precipitation threshold (Ebert, 2007). For this purpose, multiple monthly precipitation thresholds have been considered to calculate the statistics: 1, 5, 10, 20, 50 and 100 mm. Fig. 8 shows the results of the performance based on the categorical statistics. The POD (Fig. 8a) ranges between 0.8 and 1 for low precipitation values (1, 5 and 10 mm thresholds) considering all the months and both warm and cold seasons. This good performance is observed also for large precipitation values during the cold season, with stabilization around POD = 0.75; nevertheless, during the warm season the performance for large precipitation totals shows POD values lower than 0.1 for the 100 mm threshold (Fig. 8a). The behavior of the FAR shows an increase as the precipitation threshold increases, with larger values for the warm season in comparison to the cold season, particularly for the months with precipitation larger than 100 mm (Fig. 8b). In this sense, 80% of the precipitation detections above 100 mm during the warm season were incorrect, with most of these events occurring over Cuyo region. The ETS shows that the maximum detection skill during the warm season was achieved for a threshold of 20 mm, with a value of 0.23 (Fig. 8c), with almost no skill for precipitation exceeding 100 mm. Considering all the months, precipitation thresholds exceeding 20 mm shows the best detection skill, with a value closer to 0.3. The best performance is observed during the cold season for monthly precipitation higher than 20 mm (ETS ~ 0.4). A similar behavior is observed for the HSS, although with larger values for this categorical metric (Fig. 8d). Performance evaluated through the HK score indicates a low skill for all the thresholds, with negative values for higher monthly precipitation totals, i.e. performance inferior to a random estimation (Fig. 8e). Regarding the FBI, it can be observed an overestimation of precipitation totals in all the thresholds, considering all the months and the cold season (Fig. 8f). For the thresholds between 5 and 20 mm, the warm season shows the largest overestimations, while the cold season shows the lower overestimations. For thresholds of 50 and 100 mm there is an opposite seasonal behavior in the FBI, with large overestimation during the cold season and underestimation of precipitation totals during the warm season.

4.6. Precipitation performance at different elevation

Given the complex topography of the CAA, this study assessed the dependence of CHIRPS's performance on elevation. In order to achieve this, the rain gauges were classified in five groups considering their elevation: 0–700 m (10 stations), 700–1000 m (9 stations), 1000–1300 m (13 stations), 1300–1500 m (13 stations), and > 1500 m (12 stations) (see Table 1). The results for the continuous validation statistics are shown in Table 5. For the PCC, NS and PB, stations located between 700 and 1000 m.a.s.l. showed the best performance, while the MAE shows lower values for the stations located at elevations lower than 700 m. As the elevation increase, the statistics indicate that the performance of CHIRPS tends to decrease. For example, the lower PCC and NS are observed for the stations located above 1500 m (Table 5). Nevertheless, the higher values in MAE and PB are observed for the stations located between 1000 and 1300 m. In order to complement these results, we plotted the categorical POD, FAR, HSS and FBI statistics for the five selected elevation ranges and different thresholds to identify precipitation (Fig. 9). The best performance considering the POD is observed in the stations located between 1000 and 1300 m, with values between 0.8 and 1 (Fig. 9a). This behavior resembles the result obtained for the POD of the winter season (Fig. 8), which is typically the rainy season over the stations located at this altitude. Higher differences in POD for each altitude range are observed for thresholds higher than 50 mm, with the worst performance observed for precipitation higher than 100 mm in the stations located between 0 and 700 m. Nevertheless, the FAR for this group of stations shows the best performance for all the selected thresholds (Fig. 9b). Higher FAR values are observed for the stations located at higher altitudes. The HSS shows that the best performance is observed for the stations located between 0 and 1000 m, particularly for thresholds of 10 and 20 mm (Fig. 9c). The group of stations located between 1000 and 1300 m have the best performance for precipitation higher than 100 mm. Finally, the FBI shows precipitation overestimation for the stations located over 1000 m for all the selected thresholds (Fig. 9d). Underestimation of precipitation totals is observed for the stations located below 1000 m, considering a threshold higher than 50 mm. This result is in line with the findings observed in Fig. 8f, given that the rainy season of the stations located at lower elevations is recorded during summer. Additionally, large positive FBI is observed for the stations located between 1000 and 1300 m, particularly for high precipitation thresholds, a result that is mainly associated to winter precipitation totals.

4.7. Temporal evolution of regional precipitation

In order to illustrate the temporal behavior of observed and estimated precipitation, the time series of the 57 locations were averaged considering its rainy season (see Fig. 4a for the spatial distribution). This allowed to obtain two regionally-averaged time series comprising the stations that have higher precipitation amounts during the warm and cold seasons. Even when this clustering seems arbitrary, it is physically meaningful given that separates one of the main features of precipitation over the CAA. Fig. 10 show the comparison of the regionally-averaged time series of observed and estimated precipitation, together with the difference between the time series for each region. Precipitation variability at the stations with warm season maximum shows that the peaks in precipitation are not appropriately represented

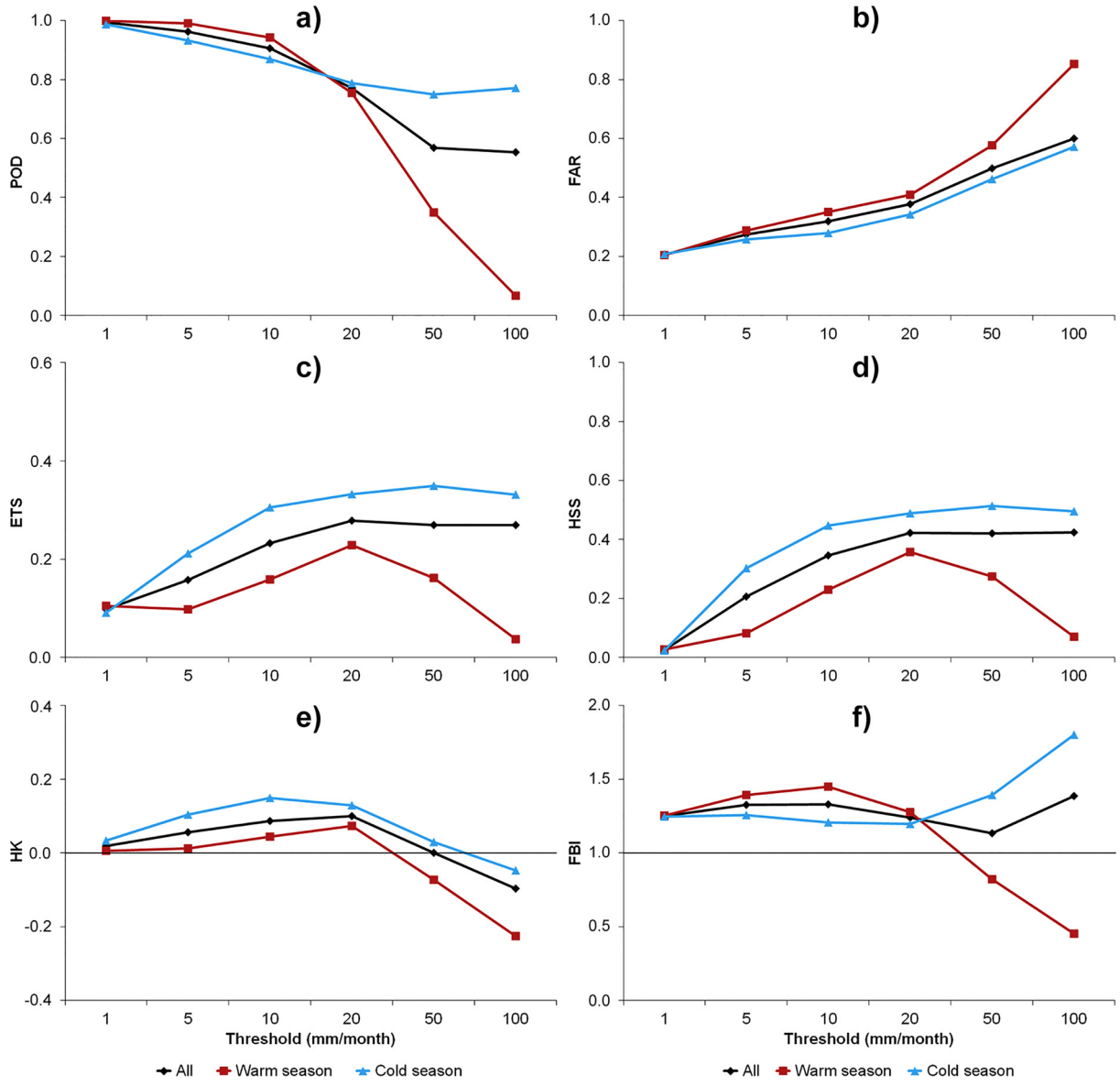

Fig. 8. Categorical verification of monthly CHIRPS precipitation estimates for the complete period and during the warm and cold seasons over the CAA as a function of the threshold value chosen to separate the precipitation/no-precipitation events: a) probability of detection, b) false alarm rate, c) equitable threat score, d) Hanssen-Kuipers discriminant, e) Heidke skill score and f) frequency bias index.

Table 5
Performance of the continuous validation statistics as a function of different elevation.

	Elevation categories (m.a.s.l.)				
Continuous metrics	0–700	700–1000	1000–1300	1300–1500	> 1500
PCC	0.708	0.744	0.715	0.606	0.470
MAE	14.464	16.008	33.653	26.077	24.353
NS	0.466	0.520	0.133	−0.149	−0.377
PB	−19.560	6.678	64.477	30.158	34.640

by CHIRPS, with an underestimation of the precipitation amounts mostly during the warm season (Fig. 10a). It was observed that in several years the magnitude of this dry bias was higher than 50 mm (1994, 1997, 1998, 2007 and 2014), representing almost half of the precipitation accumulated during the summer season over the region. Nevertheless, there is a good agreement between both regional observations and CHIRPS estimations (PCC = 0.86), with a PB of −11% and a MAE of 15.3 mm. Considering the time series of the stations with precipitation peak during the cold season, Fig. 10b shows that the annual cycle is accurately captured by CHIRPS estimations (PCC = 0.82), even in the years where a double maximum in precipitation was observed (see for example the years 1999 and 2001; Fig. 10b). However, the difference between observations and estimations shows a wet bias that is mostly evident during the cold season, with values that can be larger than 100 mm especially during the months of May of 1992, 1993, 1999, 2001, 2005, 2012 and 2016. The large values of precipitation estimated by CHIRPS during the month of May are in line with the extremes of Fig. 4b in La Jaula and Auquinco stations during this particular month (see the whisker above the quartiles). Just in few months the CHIRPS estimations showed a dry bias, a result that is in line with the PB statistic for this region considering the complete period of analysis (PB = 65.8%).

Considering Fig. 10, we focused mainly on the assessment of precipitation bias during the rainy season, which is usually translated to an annual precipitation bias as observed in Figs. 3 and 5. Nevertheless, during the dry season CHIRPS estimations show precipitation occurrences in most of the months, with just few cases of zero precipitation

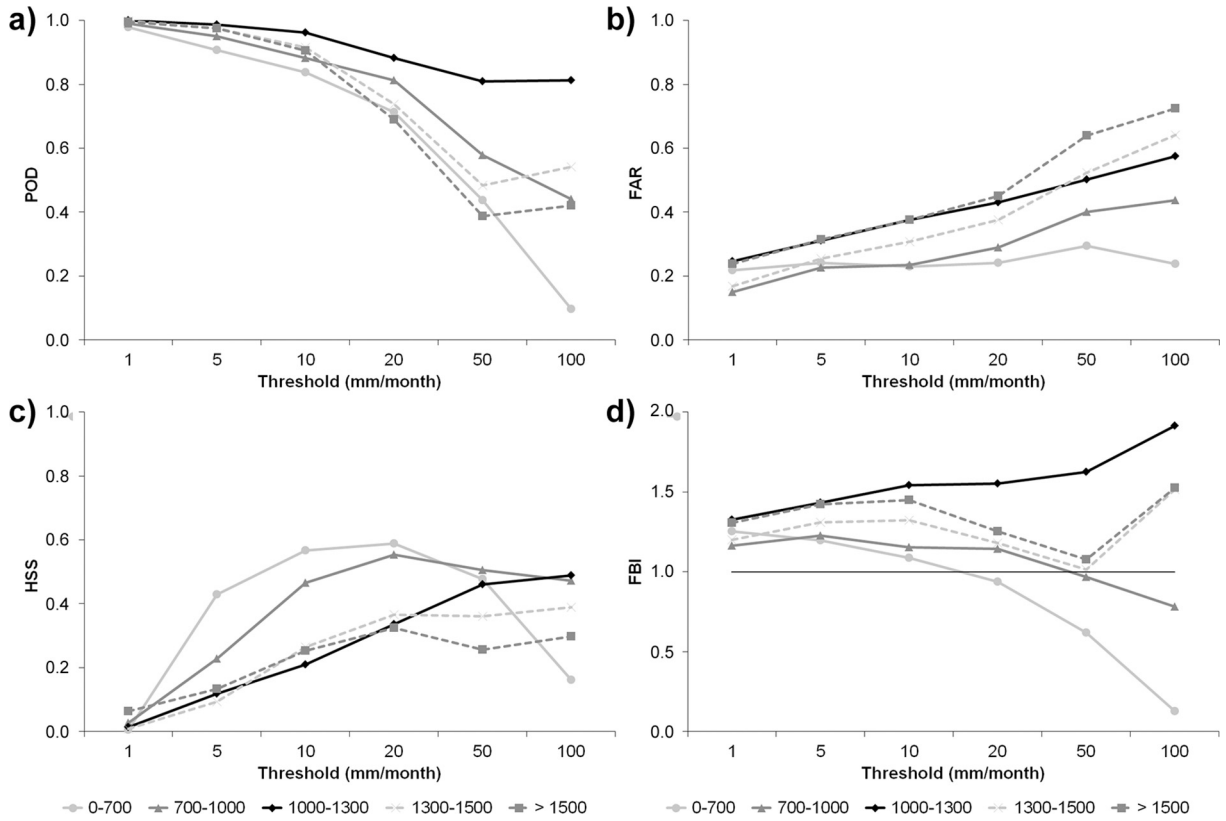

Fig. 9. Categorical metrics performance at different elevations as a function of the threshold value chosen to separate the precipitation/no-precipitation events: a) probability of detection, b) false alarm rate, c) Heidke skill score and d) frequency bias index.

during the 30 years period. This characteristic arise from a screening procedure developed to remove "false zeros" in the CHIRPS estimations, given that national and global precipitation datasets have a substantial number of values that have been incorrectly reported as zeros (Funk et al., 2014). Similar results have been previously reported over Cyprus (Katsanos et al., 2016b) and Chile (Zambrano et al., 2017).

5. Discussion

The point-to-pixel comparison of monthly precipitation data from 57 rain gauges over the CAA with the relatively new CHIRPS dataset allowed to identify its accuracy for estimating the amount, timing and spatial distribution of regional precipitation. This dataset is unique regarding spatial resolution (0.05°) and allows the study of precipitation variability for the past 37 years in high resolution. Given the lack of rain gauges and the complexity of the Andes range, accurate estimations of precipitation gradients by interpolation methods can be affected by large uncertainties. The CHIRPS precipitation dataset blends in more station data than other products and uses a high-resolution background climatology, providing better estimates of precipitation means and variations, resulting in a better hydrologic state (Shukla et al., 2014). Our results showed that the validation statistics indicated a relatively good agreement between the CHIRPS precipitation estimates and ground precipitation measurements over the CAA. However, a large wet bias (PB = 65.8%) was observed in monthly precipitation totals especially over the region where the seasonal cycle of precipitation has a maximum during the cold season (North Patagonia, western and southern Cuyo). The annual cycle and the interannual variability of precipitation over North Patagonia was accurately represented by CHIRPS estimations (PCC = 0.82), but an overestimation of precipitation during the wet season (cold semester) resulted in large errors (MAE = 34.7 mm) particularly for high precipitation totals.

One of the causes of this discrepancy between observed and estimated precipitation can be associated to the number of anchor stations used in the creation of CHIRPS, which was shown in section 2 as a deficient aspect in the generation of the product and highlights this assessment as an independent validation. Another source of uncertainty was the duplication of data from different sources. We observed that several anchor stations were included from global datasets like the Global Summary of the Day (GSOD) and the Global Historical Climatology Network (GHCN) with the same name but with different location. As an example, during March 2010 we found that data from San Juan and Neuquén stations was duplicated from these two global datasets. Considering San Juan station, coordinates from GHCN are 31.5° S, 68.699° W, elevation of 630 m; while GSOD data shows that location is 31.4° S, 68.417° W, with an elevation of 597 m. In the case of Neuquén station, GHCN data has a location in 39° S, 68.27° W with an elevation of 270 m; while the coordinates from GSOD data are 38.95° S, 68.13° W, elevation of 273 m. The information for this example can be accessed at ftp://ftp.chg.ucsb.edu/pub/org/chg/products/CHIRPS-2.0/diagnostics/monthly_station_data/2010.03.csv, and the following link has the information about the monthly station data for the complete CHIRPS period: ftp://ftp.chg.ucsb.edu/pub/org/chg/products/CHIRPS-2.0/diagnostics/monthly_station_data/. For CHIRPS calculation, stations were only added to the anchor list if they were outside of a 10-km radius from any station already in the list, assuming that stations within the 10-km radius to be duplicates (Funk et al., 2014). In this sense, a difference in the location of the rain gauges depending on the data source could led to a deficient blending, resulting in a misrepresentation of precipitation based on CHIRPS estimates.

Finally, another cause that can led to the overestimation of CHIRPS over North Patagonia region can be related to the precipitation estimates based on infrared cold cloud duration observations. In a validation of daily satellite precipitation estimates over South America, Salio et al. (2015) found that the greatest difficulties for these products to reproduce the main features of precipitation were shown to arise in

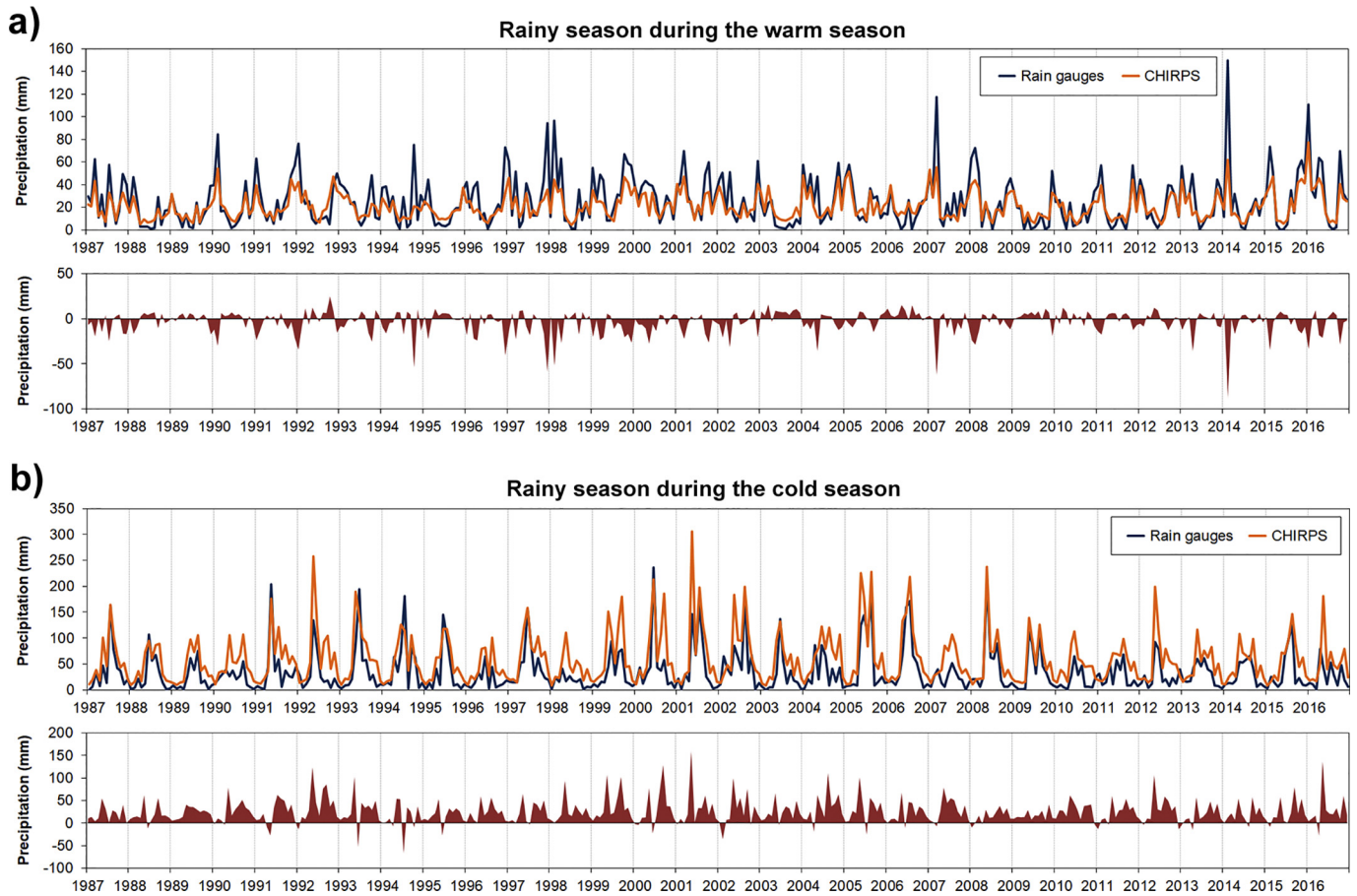

Fig. 10. Monthly regional time series of observed and estimated precipitation for the period 1987–2016. The difference between observations and CHIRPS is also presented. a) average of stations with rainy season during the warm season, b) average of stations with rainy season during the cold season.

mountainous areas and in non-convective precipitation events, features present over North Patagonia region during the rainy season. Moreover, the overestimation generated by evaporation of precipitation below the cloud base before reaching the surface, a condition present in arid to semi-arid regions like the study area (Hobouchian et al., 2017), could be playing a major role in the performance of CHIRPS estimations. Further studies are needed to quantify in detail these possible sources of error, for which observations at higher altitudes will be necessary to provide a proper characterization of precipitation over the study area.

6. Conclusions

We performed a validation of CHIRPS precipitation dataset along the Central Andes of Argentina with monthly data that covers a recent period of 30 years (1987–2016). This kind of validation is unprecedented in the study area given the number of rain gauges used and the available period of records for a satellite product. This study used observations from at least 45 rain gauges not included as anchor stations for the calculation of CHIRPS estimations, therefore it can be considered an independent validation.

CHIRPS estimations reproduce adequately several characteristics of precipitation along the CAA as the seasonal and interannual variability and the spatial patterns of precipitation. In general, the ability of CHIRPS data to capture the seasonal precipitation totals is higher in the rainy season rather than in the dry season. This dataset shows a slight underestimation (PB = −11%) of precipitation along Cuyo region, particularly associated to the areas where the rainy season takes place during the warm semester. However, there is a wet bias over North Patagonia region (PB = 65.8%) as a consequence of an overestimation of precipitation mainly during the wet season –cold semester-, leading to an average mean absolute error larger than 34 mm. Over the rainiest locations of North Patagonia, the overestimation of the higher values of precipitation can be larger than 100 mm per month, showing that the performance of CHIRPS is dependent on the representation of the dominant precipitation systems. Moreover, the complexity of the topography can introduce uncertainties in precipitation estimations that the blending with stations could not reduce, given the limited number of anchor stations used in the construction of CHIRPS. In this sense, stations located above 1000 m.a.s.l. showed the lowest performance in most of the validation statistics, although precipitation detection is accurately captured. The use of the freely available data from the SSRH in the blending procedure could improve the final CHIRPS product, although the number of rain gauges is still scarce for the study area.

In general, the CHIRPS dataset, conceived primarily to support agricultural drought monitoring, is a promising tool to assess precipitation variability over the CAA and particularly over Cuyo region. This semi-arid region is vulnerable to climate variability, ranging from drought conditions that generate wildfires to extreme precipitation events that produce landslides and debris flows over the Andes. In this sense, a continuous observing system updated regularly is essential to monitor precipitation variations over Cuyo. Drought monitoring over this region was traditionally based on the SPI (Penalba and Rivera, 2016). The use of the SPI with the CHIRPS estimations –a combination recently applied over Africa (López-Carr et al., 2014); Chile (Zambrano et al., 2017) and Southeast Asia (Guo et al., 2017)- can contribute to improve flood and drought monitoring and understanding with an adequate spatial detail and over a variety of time scales, likely leading to enhanced climate services for water managers and agricultural planners.

Acknowledgements

This work was supported by the National Agency for Scientific and Technological Promotion (ANPCyT) [grant number PICT-2016-0431]. We thank Subsecretaría de Recursos Hídricos de Argentina and Servicio Meteorológico Nacional for providing the precipitation records used in the study.

References

Aghakouchak, A., Mehran, A., Norouzi, H., Behrangi, A., 2012. Systematic and random error components in satellite precipitation data sets. Geophys. Res. Lett. 39, L09406. http://dx.doi.org/10.1029/2012GL051592.

Ahmadalipour, A., Moradkhani, H., Yan, H., Zarekarizi, M., 2017. Remote sensing of drought: vegetation, soil moisture, and data assimilation. In: Lakshmi, V. (Ed.), Remote Sensing of Hydrological Extremes. Springer, Switzerland, pp. 121–149.

Alexandersson, H., 1986. A homogeneity test applied to precipitation data. J. Climatol. 6, 661–675.

Beck, H.E., Vergopolan, N., Pan, M., Levizzani, V., van Dijk, A.I.J.M., Weedon, G., Brocca, L., Pappenberger, F., Huffman, G.J., Wood, E.F., 2017. Global-scale evaluation of 23 precipitation datasets using gauge observations and hydrological modeling. Hydrol. Earth Syst. Sci. 21, 6201–6217.

Biles, J.J., Cobos, D., 2007. Natural disasters and their impact in Latin America. In: Stoltman, J.P., Lidstone, J., DeChano, L.M. (Eds.), International Perspectives on Natural Disasters: Occurrence, Mitigation, and Consequences. Springer, Dordrecht, The Netherlands, pp. 281–302.

Boulanger, J.P., Aizpuru, J., Leggieri, L., Marino, M., 2010. A procedure for automated quality control and homogenization of historical daily temperature and precipitation data (APACH). Part 1: quality control and application to the argentine weather service stations. Clim. Chang. 98, 471–491.

Diem, J.E., Hartter, J., Ryan, S.J., Palace, M.W., 2014. Validation of satellite rainfall products for western Uganda. J. Hydrometeorol. 15, 2030–2038.

Dinku, T., Chidzambwa, S., Ceccato, P., Connor, S.J., Ropelewski, C.F., 2008. Validation of high-resolution satellite rainfall products over complex terrain. Int. J. Remote Sens. 29, 4097–4110.

Ebert, E., 2007. Methods for verifying satellite precipitation estimates. In: Levizzani, V., Bauer, P., Turkeds, F.J. (Eds.), Measuring Precipitation from Space – EURAINSAT and the Future. Springer, pp. 345–356.

Falvey, M., Garreaud, R., 2007. Wintertime precipitation episodes in Central Chile: associated meteorological conditions and orographic influences. J. Hydrometeorol. 8, 171–193.

Farooq Iqbal, M., Athar, H., 2018. Validation of satellite based precipitation over diverse topography of Pakistan. Atmos. Res. 201, 247–260.

Feidas, H., 2010. Validation of satellite rainfall products over Greece. Theor. Appl. Climatol. 99, 193–216.

Förster, K., Oesterle, F., Hanzer, F., Schöber, J., Huttenlau, M., Strasser, U., 2016. A snow and ice melt seasonal prediction modeling system for alpine reservoirs. Proc. IAHS 374, 143–150.

Funk, C.C., Peterson, P.J., Landsfeld, M.F., Pedreros, D.H., Verdin, J.P., Rowland, J.D., Romero, B.E., Husak, G.J., Michaelsen, J.C., Verdin, A.P., 2014. A quasi-global precipitation time series for drought monitoring. US Geol. Survey Data Series 832. http://dx.doi.org/10.3133/ds832.

Funk, C., Peterson, P., Landsfeld, M., Pedreros, D., Verdin, J., Shukla, S., Husak, G., Rowland, J., Harrison, L., Hoell, A., Michaelsen, J., 2015a. The climate hazards infrared precipitation with stations - a new environmental record for monitoring extremes. Sci. Data 2, 150066. http://dx.doi.org/10.1038/sdata.2015.66.

Funk, C., Verdin, A., Michaelsen, J., Peterson, P., Pedreros, D., Husak, G., 2015b. A global satellite-assisted precipitation climatology. Earth Syst. Sci. Data 7, 275–287.

Garreaud, R.D., 2009. The Andes climate and weather. Adv. Geosci. 22, 3–11.

González, M.H., 2013. Some indicators of interannual rainfall variability in patagonia (Argentina). In: Tarhule, A. (Ed.), Climate Variability – Regional and Thematic Patterns. InTech, Rijeka, Croatia, pp. 133–161.

Guo, H., Bao, A., Liu, T., Ndayisaba, F., He, D., Kurban, A., De Maeyer, P., 2017. Meteorological drought analysis in the lower Mekong Basin using satellite-based long-term CHIRPS product. Sustainability 9, 901. http://dx.doi.org/10.3390/su9060901.

Habib, E., Henschke, A., Adler, R., 2009. Evaluation of TMPA satellite-based research and real-time rainfall estimates during six tropical-related heavy rainfall events over Louisiana, USA. Atmos. Res. 94, 373–388.

Hobouchian, M.P., Salio, P., García Skabar, Y., Vila, D., Garreaud, R., 2017. Assessment of satellite precipitation estimates over the slopes of the subtropical Andes. Atmos. Res. 190, 43–54.

Katsanos, D., Retalis, A., Tymvios, F., Michaelides, S., 2016a. Analysis of precipitation extremes based on satellite (CHIRPS) and in situ dataset over Cyprus. Nat. Hazards 83, 53–63.

Katsanos, D., Retalis, A., Michaelides, S., 2016b. Validation of a high-resolution precipitation database (CHIRPS) over Cyprus for a 30-year period. Atmos. Res. 169, 459–464.

Le, A.M., Pricope, N.G., 2017. Increasing the accuracy of runoff and Streamflow simulation in the Nzoia Basin, western Kenya, through the incorporation of satellite-derived CHIRPS data. Water 9, 114. http://dx.doi.org/10.3390/w9020114.

Llano, M.P., Penalba, O.C., 2011. A climatic analysis of dry sequences in Argentina. Int. J. Climatol. 31, 504–513.

López-Carr, D., Pricope, N.G., Aukema, J.E., Jankowska, M.M., Funk, C., Husak, G., Michaelsen, J., 2014. A spatial analysis of population dynamics and climate change in Africa: potential vulnerability hot spots emerge where precipitation declines and demographic pressures coincide. Popul. Environ. 35, 323–339.

Maggioni, V., Sapiano, M.R.P., Adler, R.F., 2016. Estimating uncertainties in high-resolution satellite precipitation products: systematic or random error? J. Hydrometeorol. 17, 1119–1129.

Maidment, R.I., Allan, R.P., Black, E., 2015. Recent observed and simulated changes in precipitation over Africa. Geophys. Res. Lett. 42, 8155–8164.

Mantas, V.M., Liu, Z., Caro, C., Pereira, A.J.S.C., 2015. Validation of TRMM multi-satellite precipitation analysis (TMPA) products in the Peruvian Andes. Atmos. Res. 163, 132–145.

McKee, T.B., Doesken, N.J., Kleist, J., 1993. The relationship of drought frequency and duration to time scales. In: Proceedings of the Eight Conference on Applied Climatology. American Meteorological Society, Anaheim, pp. 179–184.

Nash, J.E., Sutcliffe, J.V., 1970. River flow forecasting through conceptual models part I—a discussion of principles. J. Hydrol. 10, 282–290.

Paredes-Trejo, F.J., Barbosa, H.A., Peñaloza-Murillo, M.A., Moreno, M.A., Farías, A., 2016. Intercomparison of improved satellite rainfall estimation with CHIRPS gridded product and rain gauge data over Venezuela. Atmósfera 29, 323–342.

Paredes-Trejo, F.J., Barbosa, H.A., Lakshmi Kumar, T.V., 2017. Validating CHIRPS-based satellite precipitation estimates in Northeast Brazil. J. Arid Environ. 139, 26–40.

Penalba, O.C., Rivera, J.A., 2016. Precipitation response to El Niño/La Niña events in southern South America - emphasis in regional drought occurrences. Adv. Geosci. 42, 1–14.

Penalba, O.C., Rivera, J.A., Pántano, V.C., 2014. The CLARIS LPB database: constructing a long-term daily hydro-meteorological dataset for La Plata Basin, southern South America. Geosci. Data J. 1, 20–29.

Porcù, F., Milani, L., Petracca, M., 2014. On the uncertainties in validating satellite instantaneous rainfall estimates with raingauge operational network. Atmos. Res. 144, 73–81.

Rahmawati, N., Lubczynski, M.W., 2017. Validation of satellite daily rainfall estimates in complex terrain of Bali Island, Indonesia. Theor. Appl. Climatol. http://dx.doi.org/10.1007/s00704-017-2290-7.

Rivera, J.A., Penalba, O.C., Villalba, R., Araneo, D.C., 2017. Spatio-temporal patterns of the 2010-2015 extreme hydrological drought across the Central Andes, Argentina. Water 9, 652. http://dx.doi.org/10.3390/w9090652.

Salio, P., Hobouchian, M.P., García Skabar, Y., Vila, D., 2015. Evaluation of high-resolution satellite precipitation estimates over southern South America using a dense rain gauge network. Atmos. Res. 163, 146–161.

Santos, J.R., Norte, F., Moreiras, S., Araneo, D., Simonelli, S., 2015. Predicción de episodios de precipitación que ocasionan aludes en el área montañosa del noroeste de la provincia de Mendoza. Argentina. Geoacta 40, 65–75.

Schwerdtfeger, W., 1976. The atmospheric circulation over Central and South America. In: Schwerdtfeger, W. (Ed.), Climates of Central and South America. Elsevier, New York, USA. Vol. 2. pp. 2–12.

Seoane, R.S., Valdés, J.B., Mata, L.J., 2005. Climate variability and climate change in Patagonian rivers. In: Wagener, T. (Ed.), Regional Hydrological Impacts of Climatic Change – Impact Assessment and Decision Making. Vol. 295. IAHS Publication, Wallingford, UK, pp. 26–36.

Shukla, S., McNally, A., Husak, G., Funk, C., 2014. A seasonal agricultural drought forecast system for food-insecure regions of East Africa. Hydrol. Earth Syst. Sci. 18, 3907–3921.

Tang, L., Tian, Y., Yan, F., Habib, E., 2015. An improved procedure for the validation of satellite-based precipitation estimates. Atmos. Res. 163, 61–73.

Tencer, B., Rusticucci, M., Jones, P., Lister, D., 2011. A southeastern South America daily gridded dataset of observed surface minimum and maximum temperature for 1961-2000. Bull. Am. Meteorol. Soc. 92, 1339–1346.

Thiemig, V., Rojas, R., Zambrano-Bigiarini, M., Levizzani, V., De Roo, A., 2012. Validation of satellite-based precipitation products over sparsely gauged African River basins. J. Hydrometeorol. 13, 1760–1783.

Toté, C., Patricio, D., Boogaard, H., Van Der Wijngaart, R., Tarnavsky, E., Funk, C., 2015. Evaluation of satellite rainfall estimates for drought and flood monitoring in Mozambique. Remote Sens. 7, 1758–1776.

Viale, M., Norte, F., 2009. Strong Cross-Barrier Flow under Stable Conditions Producing Intense Winter Orographic Precipitation: A Case Study over the Subtropical Central Andes, Wea. Forecast. 24, 1009–1031.

Viale, M., Nuñez, M.N., 2011. Climatology of winter orographic precipitation over the subtropical Central Andes and associated synoptic and regional characteristics. J. Hydrometeorol. 12, 481–507.

Vigaud, N., Lyon, B., Giannini, A., 2017. Sub-seasonal teleconnections between convection over the Indian Ocean, the east African long rains and tropical Pacific surface temperatures. Int. J. Climatol. 37, 1167–1180.

Willmott, C.J., 1981. On the validation of model. Phys. Geogr. 2, 184–194.

Willmott, C.J., Robeson, S.M., Matsuura, K., 2017. Climate and other models may be more accurate than reported. Eos 98. http://dx.doi.org/10.1029/2017EO074939.

Zambrano, F., Wardlow, B., Tadesse, T., Lillo-Saavedra, M., Lagos, O., 2017. Evaluating satellite-derived long-term historical precipitation datasets for drought monitoring in Chile. Atmos. Res. 186, 26–42.

Zambrano-Bigiarini, M., Nauditt, A., Birkel, C., Verbist, K., Ribbe, L., 2017. Temporal and spatial evaluation of satellite-based rainfall estimates across the complex topographical and climatic gradients of Chile. Hydrol. Earth Syst. Sci. 21, 1295–1320.